Cationic surface segregation in doped LaMnO₃

V. Sharma · M. K. Mahapatra · P. Singh ·
R. Ramprasad

Abstract The surface cation chemistry in (La, A)MnO₃ (A = Ca, Sr and Ba) is investigated using first-principles thermodynamics. We find that, all three dopants tend to segregate to the surface over a wide range of T–p_{O_2} conditions and the tendency for segregation increases with the increase in the dopant cationic size. Moving toward the low oxygen pressure, dopants prefer to remain in the surface regions accompanied by the appropriate number of charge compensating oxygen vacancies. The situation when dopants remain in the bulk regions tends to occur close to the thermodynamic conditions that also favor the decomposition of LaMnO₃. The present work serves as an important step toward understanding of factors governing the cationic surface segregation in doped LaMnO₃ and opens a pathway to study other important chemical environments (such as water- and CO₂-containing air) which are crucially given the fact that the 'real-world' air enhances cationic segregation.

Introduction

Mixed metal perovskite oxides such as (La, A)MnO₃ and (La, A)CoO₃ are commonly found in several catalytic and

V. Sharma (✉) · M. K. Mahapatra · P. Singh · R. Ramprasad
Materials Science and Engineering, University of Connecticut, Storrs, CT, USA
e-mail: vinit.sharma.mlsu@gmail.com; vinit.sharma@uconn.edu

V. Sharma · R. Ramprasad
Institute of Materials Science, University of Connecticut, Storrs, CT, USA

M. K. Mahapatra · P. Singh
Center for Clean Energy Engineering, University of Connecticut, Storrs, CT, USA

electrochemical devices, for example, as cathodes in solid oxide fuel cells (SOFCs) [1–4]. In these compounds, A is a metal atom dopant (typically with lower valence than La) that partially substitutes La atoms in the parent LaMnO₃ and LaCoO₃ materials. Under the prevailing oxygen-rich and moisture-rich conditions that such oxides encounter in typical SOFCs, preferential segregation of the A atoms to the surfaces is commonly observed [3, 5–10]. This surface segregation is detrimental to the overall performance as it leads to reduced oxygen reduction activity and cathode stability [1, 2]. The slow rate of oxygen reduction reaction (ORR), which is generally agreed to be limited by the surface exchange reactions on conducting cathodes, imposes the main barrier for implementation of high-performance SOFCs. To attain highly reactive and stable cathode surfaces for fast ORR kinetics, it is important to tailor the catalytic activity of transition metal oxide cathode with a thorough knowledge of the surface composition and structure at the atomic level. The structure and chemistry are driven dynamically by the surrounding environments at a given temperature–pressure conditions. Although experimental [3, 5–10] and computational [3, 5, 8–13] studies have attempted to explain the cation segregation, in terms of the formation of cation-containing phases [14, 15], and charge compensation [6, 16], a detailed study to determine the impact of 'real-world' conditions (e.g., T– p_{O_2} conditions) on segregation is required.

In the present contribution, we utilize a first-principles thermodynamic analysis to assess (a) the tendency for M atom surface segregation in (La, A)MnO₃, with A being Ca, Sr, and Ba dopants, (b) the effects of oxygen pressure during annealing on the surface chemistry in typical SOFCs operating conditions and (c) role of the oxygen vacancy concentration. We assume that the (La, A)MnO₃

(001) surface is exposed to an oxygen reservoir, and identify the temperature (T) and oxygen pressure (p_{O_2}) conditions that favor cationic surface segregation. The concentration of oxygen vacancies that would accompany such segregation (or lack thereof) was also explicitly included in this treatment. We find that, while all three dopants tend to segregate to the surface over a wide range of T–p_{O_2} conditions, the tendency for segregation is directly related to the dopant cationic size. For the dopants considered, it is only at rather low p_{O_2} or high T (close to conditions that favor LaMnO$_3$ decomposition) that surface segregation is suppressed. Under these conditions, the dopant prefers to remain in the bulk regions accompanied by the appropriate number of charge compensating oxygen vacancies. The favorable agreement of the identified cationic surface segregation behaviors for the chosen dopants with available experimental data is indicative of the usefulness of such first-principles thermodynamic approaches, which can be used next to study other more involved and relevant situations (e.g., surface segregation of a larger variety of dopants in the presence of moisture) [14, 15].

Computational and model details

Our first-principles density functional theory (DFT) calculations were performed using the Vienna ab initio simulation package (VASP) [17–19], with the electronic exchange–correlation interaction treated within the generalized gradient approximation using the Perdew-Burke-Ernzerhof semilocal functional [20]. The projector augmented wave (PAW) method is used to describe the ionic cores with a plane wave expansion cutoff of 400 eV. Geometries were relaxed using a conjugate gradient algorithm until the forces on all unconstrained atoms became smaller than <0.03 eV/Å. Appropriate Monkhorst–Pack k-point meshes were considered to produce results with an energy convergence of 0.5 meV/atom. The optimized lattice parameter of the bulk cubic LaMnO$_3$ (3.91 Å) is slightly overestimated with respect to available experimental results (3.89 Å) [21]. The overestimation of lattice parameters is also observed in earlier DFT based studies [22, 23] and can be explained in terms of formation of high spin state of Mn.

The procedure adopted in the present study to arrive at our conclusions is schematically captured in Fig. 1. Our reference system, shown in the left of Fig. 1, is a LaMnO$_3$ slab with two La atoms substituted with two A atoms in the interior (i.e., the "bulk" region) of the slab. Our goal is to determine the propensity of this reference system to transform to either a situation with the La atoms at the surface (accompanied by a certain number of O vacancies), or to a situation with the La atoms remaining in the bulk
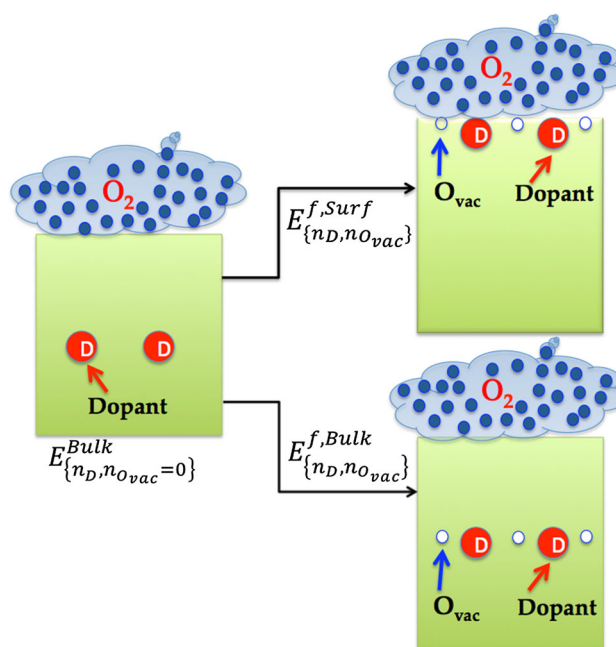

Fig. 1 Schematic representation of the surface segregation of dopants in (La, A)O-terminated (A = Ca, Sr and Ba) slab. Dopants and oxygen vacancies are shown in *red* and *blue* (*open*) *spheres*, respectively. *Left* part of the figure is our reference system composed of a LaMnO$_3$ slab with two La atoms substituted with two A atoms (without any O vacancy, $n_{O_{vac}} = 0$) in the bulk region of the slab (Color figure online)

region (accompanied by O vacancies). These two considered outcomes are shown in the right of Fig. 1. It is assumed that the surface is in contact with a gas phase reservoir of O$_2$.

It has been already established that under typical SOFCs operational conditions, doping makes (La, A)O termination favorable [11]. The cationic surface segregation behavior is examined using a 5-layer stoichiometric slab with (La, A) O-termination (001) surface, as shown in Fig. 2. Two La atoms are substituted at a time with Ca, Sr, or Ba, either in the central LaO plane, or in the surface LaO plane, corresponding to a dopant concentration of ∼7.4 %. Slabs are separated by a vacuum spacing of 16 Å, chosen by testing the variation in total energy with vacuum distance and the decay of the local potential away from the surfaces. We adopt 5-layer stoichiometric slabs after considering the tradeoff between the energetic convergences and the amount of computation time. The difference between segregation energies computed using a 5-layer and a 9-layer La(Sr)O-terminated slab was negligible (<0.01 eV), indicating that for our purposes a 5-layer slab is thick enough. In our considered 5-layer model, the bottom three layers were fixed to simulate the bulk region, hence we have considered the dopant segregation toward topside of the surface.

All the calculations are performed using a (3 × 2) surface unit cell. The choice of two dopant atoms replacing
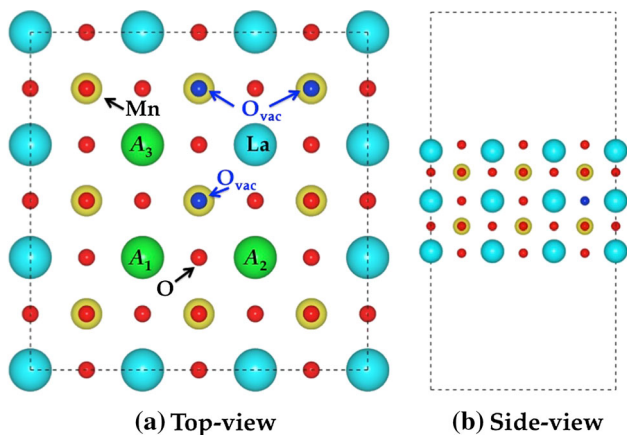
Fig. 2 *Top-view* and *side-view* of the (La, *A*)O-terminated (001) surface model, where *A* = Ca, Sr, and Ba. Several possible bulk and surface structures with two dopants (*A*) at a time along with a range of O vacancies (O_{vac}) starting from 0 to 3 are considered. The host atoms sites La, Mn, and O are shown as *sky blue*, *yellow*, and *red spheres*, respectively. The possible dopant substitution (A_1, A_1, and A_3) and O_{vac} sites are shown in *green* and *blue spheres*, respectively (Color figure online)

two La atoms at a time was motivated by the fact that the nominal oxidation state of La is +3 and that of the dopants is +2, implying that replacement of two La atoms by two dopant atoms will lead to a charge imbalance that can be compensated by one O vacancy. In addition, for each case of dopant and for each case of dopant locations, n_{Ovac} O vacancies were considered (with n_{Ovac} = 0–3). Several configurations of the dopant atoms and the O vacancies in the vicinity of the dopants were considered. As the lowest-energy sites occur in the neighborhood of the dopant [24], all possible first and second neighboring O vacancy sites were considered. The top and side views of the representative model indicating the dopant substitution and O vacancy sites are shown in Fig. 2.

Due to the errors associated with the on site Coulomb and exchange interactions [25], DFT-based methods are known to fail to reproduce an accurate description of the electronic structure for strongly correlated systems such

as late transition metal oxides [26, 27] and rare-earth compounds [28]. In such cases, the accuracy of DFT can be improved by incorporating a Hubbard-model-type correction (*U*), which accounts for localized *d* and *f* orbitals. To investigate the effects of the *U* value, we have calculated the O vacancy formation energies of $LaMnO_3$ and (La, *A*)MnO_3 using the DFT + *U* approach with the optimal *U* values of 4 and 6 eV. The calculated O vacancy formation energies in (La, *A*)MnO_3 when the vacancy is in the bulk and at the surface are shown in Fig. 3a, b. A value of *U* = 6 eV has been shown in the past to reproduce the correct electronic structure and O vacancy formation energy of $LaMnO_3$ [23, 26]. Hence, in the present work, all the calculations are preformed using *U* = 6 eV.

Results and discussion

Referring to the processes schematically shown in Fig. 1, the formation energy, $E^{f,\text{Surf/Bulk}}_{\{n_D, n_{O_{vac}}\}}$, of the system with the n_D dopants and $n_{O_{vac}}$ O vacancies at the surface or the bulk (with respect to the reference system in which just the n_D dopants are in the bulk region) is defined as

$$E^{f,\text{Surf/Bulk}}_{\{n_D, n_{O_{vac}}\}} = \left(E^{\text{Surf/Bulk}}_{\{n_D, n_{O_{vac}}\}} - E^{\text{Bulk}}_{\{n_D, n_{O_{vac}}=0\}}\right) + \frac{n_{O_{vac}}}{2}\mu O_2, \quad (1)$$

where $E^{\text{Surf/Bulk}}_{\{n_D, n_{O_{vac}}\}}$ is the DFT total energy of the system with n_D dopants and $n_{O_{vac}}$ O vacancies at the surface or the bulk. Throughout this work, as mentioned above, n_D = 2. μO_2 is the chemical potential of the oxygen given by

$$\mu O_2(T, p_{O_2}) = E^{\text{DFT}}_{O_2} + \Delta\mu_{O_2}(T, p_{O_2}), \quad (2)$$

where $E^{\text{DFT}}_{O_2}$ is the DFT energy of an isolated O_2 molecule. $\Delta\mu_{O_2}$ includes contributions from the translational, rotational, and vibrational degrees of freedom of the O_2 molecule, and can be determined via statistical thermodynamics or from thermochemical JANAF Tables [29]. Combining Eqs. (1) and (2) leads us to

Fig. 3 O vacancy formation energies of (La, *A*)MnO_3, where *A* is Ca, Sr, and Ba, when dopants are at the **a** bulk and **b** surface for different choices of *U* (in eV)
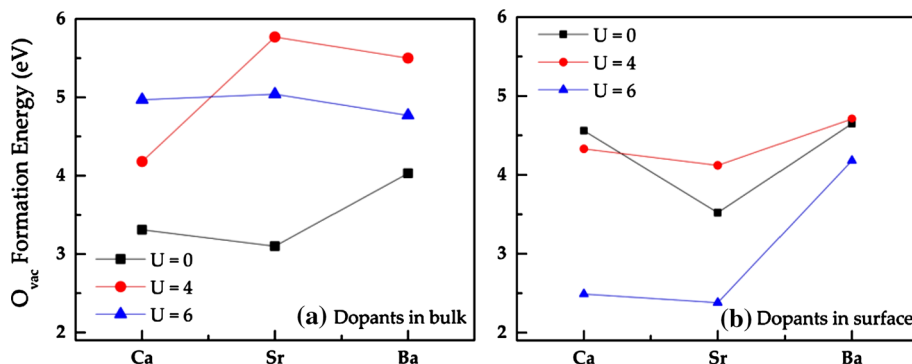
Table 1 Calculated values of $\Delta E^{f,\mathrm{Surf/Bulk}}_{\{n_D,n_{O_{vac}}\}}$ (the term in the square brackets of Eq. 3), as a function of $n_{O_{vac}}$ with $n_D = 2$ (i.e., two dopants in the bulk or at the surface). The energy of the slab with two dopants in the bulk region (with $n_{O_{vac}} = 0$) is considered as reference

Dopants	$\Delta E^{f,\mathrm{Surf/Bulk}}_{\{n_D=2,n_{O_{vac}}\}}$ (eV)							
	$n_{O_{vac}}$ (in bulk)				$n_{O_{vac}}$ (on surface)			
	0	1	2	3	0	1	2	3
Ca	0	4.97	10.06	14.14	−0.06	2.49	7.9	12.89
Sr	0	5.04	8.82	14.42	−0.17	2.38	7.67	11.51
Ba	0	4.77	9.86	13.94	−0.26	4.18	8.68	14.34

$$E^{f,\mathrm{Surf/Bulk}}_{\{n_D,n_{O_{vac}}\}} = \left[E^{\mathrm{Surf/Bulk}}_{\{n_D,n_{O_{vac}}\}} - E^{\mathrm{Bulk}}_{\{n_D,n_{O_{vac}}=0\}} + \frac{n_{O_{vac}}}{2} E^{\mathrm{DFT}}_{O_2} \right] + \frac{n_{O_{vac}}}{2} \Delta\mu_{O_2}(T, p_{O_2}). \tag{3}$$

The terms in square brackets (referred to henceforth as $\Delta E^{f,\mathrm{Surf/Bulk}}_{\{n_D,n_{O_{vac}}\}}$) are the 0 K formation energy, and can be evaluated purely using DFT calculations (provided the entropic contribution of the condensed phases can be ignored). The last term provides the T and p_{O_2} dependence arising from the gas phase. Table 1 contains $\Delta E^{f,\mathrm{Surf/Bulk}}_{\{n_D,n_{O_{vac}}\}}$ for different choices of dopants and number of O vacancies. Although we have considered a number of dopant and/or O vacancy configurations, only the energies of the most favored configuration for each case are reported in Table 1.

Equation (3), along with the data of Table 1, may be used to determine the thermodynamic preference of various scenarios as a function of $\Delta\mu_{O_2}$, as portrayed in Fig. 4 for each case of dopants, and for each choice of $n_{O_{vac}}$ (and with

$n_D = 2$ in all cases, of course). The dopants and O vacancies are either in the bulk region (solid lines in Fig. 4) or at the surface (dashed lines). The slopes of the lines are $\frac{n_{O_{vac}}}{2}$, and hence, the horizontal lines represent the cases where O vacancies are absent. It is immediately obvious that for a range of $\Delta\mu_{O_2}$ going all the way to zero, the two dopants prefer to be at the surface (devoid of O vacancies). It is only at rather low $\Delta\mu_{O_2}$ that dopants favor the bulk (or interior) region, accompanied by one or more O vacancies. However, this desired situation tends to occur close to the thermodynamic conditions that also favor the decomposition of LaMnO₃.

The T-p_{O_2} conditions corresponding to a specific value of $\Delta\mu_{O_2}$ may be determined, as mentioned above. Figure 4 also shows p_{O_2} scales for $T = 1100$ and 1500 K. It can be seen that at prevailing pressures that SOFC systems encounter, such as $1–10^{-6}$ atm (for both choices of T), surface segregation (devoid of O vacancies) is indeed favored. Moving toward the low O_2 pressures and/or high T, the surface favors the formation of oxygen vacancies, as shown in Fig. 4. It is only at rather low O_2 pressures and/or high T that the segregation behavior is suppressed, but this regime comes close to conditions that favor decomposition of LaMnO₃ (this regime is also indicated in Fig. 4). These findings are consistent with recent experimental observations indicating that the extent of dopant segregation was largest at ∼1 atm which decreases with decreasing oxygen pressure ($\sim 10^{-12}$ atm) at 1100 K [5]. Based on this thermodynamic analysis, it can be safely concluded that surface segregation of dopants in (La, A)MnO₃ (when exposed to O_2) is an inevitable consequence of thermodynamics. The segregation energy, defined as the energy difference between the horizontal lines corresponding to bulk and
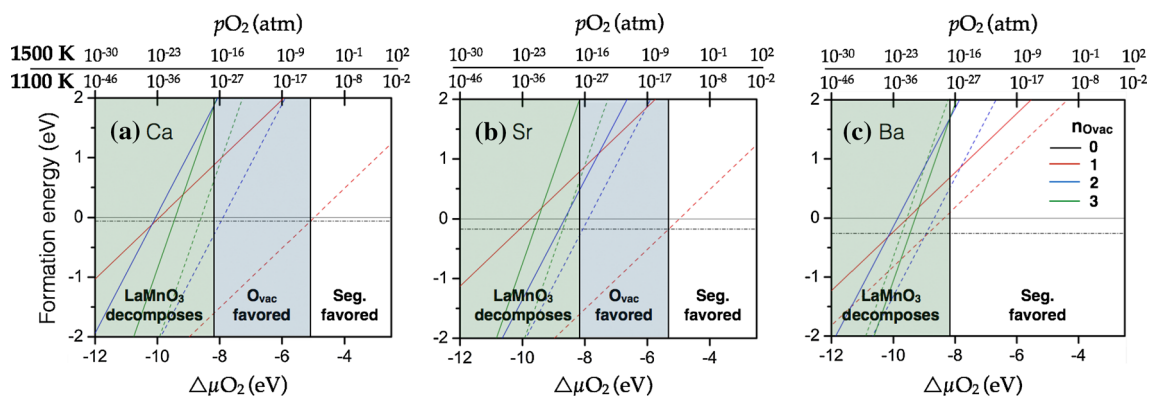

Fig. 4 The formation energies of (La, A)MnO₃, where A is **a** Ca, **b** Sr, and **c** Ba, and $n_{O_{vac}}$ O vacancies at the surface or the bulk as a function of the O_2 chemical potential. *Solids* and *dash lines* are corresponding to situation where two dopants are considered in bulk and surface region of the slab. The lines at zero represent the energies of the system with two dopants in bulk, $E^{f,\mathrm{Bulk}}_{\{n_D,n_{O_{vac}}=0\}}$ and considered as

a reference line. To capture the SOFCs operating conditions, the dependence of chemical potential of O_2 in the gas phase is translated into the pressure scales at 1100 and 1500 K. The *shaded* part represents the regions, where host material decomposes (*green*), favored the formation of $n_{O_{vac}}$ (*blue*) and segregates toward the surface (*white*) (Color figure online)

surface dopant situations, is −0.06, −0.17, and −0.26 eV/atom, respectively, for Ca, Sr, and Ba (cf. Fig. 4; Table 1), in favorable agreement with available experimental [5, 7] and ab initio results [5]. Although the segregation energies reported in this work does not include the entropic component but we believe that trend of the tendency for segregation will remain unchanged. Enrichment of the dopant in the system would result into high concentration of the dopant at the surface compared to the bulk. After a certain dopant concentration on surface segregation may lead to the formation of new phases, which in fact has been seen in experiments [5]. Here, we have not considered the surface configurations such as phase separation on surface, effect of the presence of various chemical environments such as water- and CO_2-containing air is not considered in the present study.

Next, we attempt to understand the dependence of our surface segregation energy results and trends on the type of dopant. The segregation energy for the Ca dopant is the least (and very small) and for Ba is the most. Our past experience and understanding with dopant chemistry in perovskites [24] suggest that the stability and the location of a dopant is mainly governed by the mismatch of the ionic size and oxidation state of the dopant with respect to the host atom [24]. In the present case, the nominal oxidation state of all three considered dopants is +2. Hence, it is fair to conclude that the observed variation in surface segregation is strongly dominated by the size mismatch between the dopant and host cations (La, in our case). The ionic radius of La is 1.36 Å, and that of Ca, Sr, and Ba are 1.34, 1.44, and 1.61 Å, respectively. The ionic radius of Ca is thus almost identical to that of La, correlating well with the negligible surface segregation energy for this case. The larger ionic radii of Sr and Ba lead to progressively more negative surface segregation energies, indicating that the dominant factor that controls surface segregation even in such ionic systems is the ionic size (and the tendency to minimize elastic strain energy, as alluded to recently) [5, 30]. Indeed, recent experimental work has shown that the Ca-doped $LaMnO_3$ films showed a relatively smaller amount of dopant segregation than the Sr-doped variety [5], which is consistent with our results.

Conclusions

To summarize, an attempt to understand the surface cation chemistry (La, A)MnO_3 (A = Ca, Sr, and Ba) has been made using the first-principles thermodynamic approach. It is observed that all three dopants tend to segregate to the surface over a wide range of T–p_{O_2} conditions; the tendency for segregation is directly related to the dopant cationic size. Moreover, the surface remains significantly enriched with the dopants under all realistic conditions and favors the formation of oxygen vacancies at low O_2 pressures and/or high T. The mapping of surface energetics for various La-site dopants adds to the current state of understanding aimed at modifying $LaMnO_3$ chemistry to minimize undesired cationic segregation. Further understanding in different chemical environments (such as water and CO_2 containing air) is required given the fact that the 'real-world' air enhances cationic segregation [31].

References

1. Adler SB (2004) Factors governing oxygen reduction in solid oxide fuel cell cathodes. Chem Rev 104(10):4791–4844
2. Jacobson AJ (2010) Materials for Solid Oxide Fuel Cells. Chem Mater 22(3):660–674
3. Cai Z, Kubicek M, Fleig J, Yildiz B (2012) Chemical heterogeneities on La 0.6Sr 0.4CoO3—δ thin films—correlations to cathode surface activity and stability. Chem Mater 24(6):1116–1127
4. Cai Z, Kuru Y, Han JW, Chen Y, Yildiz B (2011) Surface electronic structure transitions at high temperature on perovskite oxides: the case of strained La 0.8Sr 0.2CoO3 thin films. J Am Chem Soc 133(44):17696–17704
5. Lee W, Han JW, Chen Y, Cai Z, Yildiz B (2013) Cation size mismatch and charge interactions drive dopant segregation at the surfaces of manganite perovskites. J Am Chem Soc 135(21): 7909–7925
6. Crumlin EJ, Mutoro E, Liu Z et al (2012) Surface strontium enrichment on highly active perovskites for oxygen electrocatalysis in solid oxide fuel cells. Energy Environ Sci 5(3):6081
7. Herger R, Willmott P, Schlepütz C, et al (2008) Structure determination of monolayer-by-monolayer grown La1—xSrxMnO3 thin films and the onset of magnetoresistance. Phys. Rev. B 77(8):085401
8. Mastrikov YA, Merkle R, Heifets E, Kotomin EA, Maier J (2010) Pathways for oxygen incorporation in mixed conducting perovskites: A DFT-based mechanistic analysis for (La, Sr)MnO3—δ. J Phys Chem C 114(7):3017–3027
9. Choi SO, Penninger M, Kim CH, Schneider WF, Thompson LT (2013) Experimental and computational investigation of effect of Sr on NO oxidation and oxygen exchange for La 1—xSr xCoO3 perovskite catalysts. ACS Catal. 3(12):2719–2728
10. Jalili H, Han JW, Kuru Y, Cai Z, Yildiz B (2011) New insights into the strain coupling to surface chemistry, electronic structure, and reactivity of La 0.7Sr 0.3MnO3. J Phys Chem Lett 2(7):801–807
11. Piskunov S, Heifets E, Jacob T, et al (2008) Electronic structure and thermodynamic stability of LaMnO3 and La1—xSrxMnO3 (001) surfaces: Ab initio calculations. Phys Rev B 78(12):121406
12. Choi Y, Mebane DS, Lin MC, Liu M (2007) Oxygen reduction on LaMnO3-based cathode materials in solid oxide fuel cells. Chem Mater 19(7):1690–1699
13. Puchala B, Lee YL, Morgan D (2013) A-site diffusion in La1—xSrxMnO3: ab initio and kinetic monte carlo calculations. J Electrochem Soc 160(8):F877–F882

14. Jiang SP, Love JG (2001) Origin of the initial polarization behavior of Sr-doped LaMnO$_3$ for O$_2$ reduction in solid oxide fuel cells. Solid State Ionics 138:183–190

15. Wu Q-H, Liu M, Jaegermann W (2005) X-ray photoelectron spectroscopy of La0.5Sr0.5MnO$_3$. Mater Lett 59(12):1480–1483

16. Fister TT, Fong DD, Eastman JA et al (2008) In situ characterization of strontium surface segregation in epitaxial La[sub 0.7]Sr[sub 0.3]MnO[sub 3] thin films as a function of oxygen partial pressure. Appl Phys Lett 93(15):151904

17. Kresse G, Hafner J (1994) Ab initio molecular-dynamics simulation of the liquid-metal–amorphous-semiconductor transition in germanium. Phys Rev B 49(20):14251–14269

18. Kresse G, Furthmuller J (1996) Efficiency of ab initio total energy calculations for metals and semiconductors using a plane-wave basis set. Computational Mateials Science 6:15–50

19. Kresse G, Furthmuller J (1996) Efficient iterative schemes for ab initio total-energy calculations using a plane-wave basis set. Phys Rev B 54:11169–11182

20. Perdew JP, Burke K, Ernzerhof M (1996) Generalized gradient approximation made simple. Phys Rev Lett 77(18):3865–3868

21. Raisch C, Langheinrich C, Werner R et al (2013) X-ray photoelectron diffraction study of dopant effects in La0.7X0.3MnO$_3$ (X = La, Sr, Ca, Ce) thin films. J Appl Phys 113(6):063511

22. Akhade SA, Kitchin JR (2011) Effects of strain, d-band filling, and oxidation state on the bulk electronic structure of cubic 3d perovskites. J Chem Phys 135(10):104702

23. Su H-Y, Sun K (2014) DFT study of the stability of oxygen vacancy in cubic ABO3 perovskites. J Mater Sci

24. Sharma V, Pilania G, Rossetti GA, Slenes K, Ramprasad R (2013) Comprehensive examination of dopants and defects in BaTiO_{3} from first principles. Phys Rev B 87(13):134109

25. Anisimov VI, Aryasetiawan F, Lichtenstein AI (1997) First-principles calculations of the electronic structure and spectra of strongly correlated systems: the LDA + U method. J Phys 9:767–808

26. Lee Y-L, Kleis J, Rossmeisl J, Morgan D (2009) Ab initio energetics of LaBO_{3}(001) (B = Mn, Fe, Co, and Ni) for solid oxide fuel cell cathodes. Phys Rev B 80(22):224101

27. Jain A, Hautier G, Ong SP, et al (2011) Formation enthalpies by mixing GGA and GGA + U calculations. Phys Rev B 84(4):045115

28. Staruch M, Sharma V, Cruz dela C, Ramprasad R, Jain M (2014) Magnetic ordering in TbMn0.5Cr0.5O$_3$ studied by neutron diffraction and first-principles calculations. J Appl Phys 116(3):033919

29. Zhu H, Tang C, Ramprasad R (2010) Phase equilibria at Si-HfO_{2} and Pt-HfO_{2} interfaces from first principles thermodynamics. Phys Rev B 82(23):235413

30. Han JW, Kitchin JR, Sholl DS (2009) Step decoration of chiral metal surfaces. J Chem Phys 130(12):124710

31. Hu B, Keane M, Mahapatra MK, Singh P (2014) Stability of strontium-doped lanthanum manganite cathode in humidified air. J Power Sources 248:196–204